Transition-metal oxide pillared clays

Part 2†—A comparative study of textural and acidic properties of manganese(III) pillared montmorillonite and pillared acid-activated montmorillonite

Trilochan Mishra and Kulamani Parida*

Regional Research Laboratory, Bhubaneswar-751 013, Orissa, India

Manganese(III) pillared montmorillonite samples have been prepared by intercalating the trinuclear manganese(III) acetate complex $\{[Mn_3O(COOCH_3)_6(H_2O)_3]^+CH_3COO^-\}$ between the silicate layers of both Na-exchanged (NaMont) and acid-activated montmorillonite (HMont), and characterised by different techniques. As far as the intercalation is concerned, the multistep ion-exchange process gave better loading of the complex in comparison to the single-step process. FTIR analysis shows the presence of a bidentate acetate group inside the silicate layer which decomposes at 300 °C. Materials prepared from both clays are thermally stable up to 500 °C, with basal spacings of 17.1 and 16.9 Å and surface areas of 280 and 268 $m^2\ g^{-1}$, (NaMont, HMont respectively). Although the acid-activated pillared montmorillonite shows low uptake of the complex and low surface area, the resultant material has higher pore volume and acidity in comparison to the product from the Na-exchanged material. Samples prepared from acid-activated clays possess both micropores and mesopores (average pore diameter 41 Å) while those prepared from Na-exchanged clays show predominately uniform small pores with an average pore diameter of 33 Å.

In recent years, considerable interest has been focussed on the preparation and characterization of different types of pillared layered compounds and their possible applications as catalysts and adsorbents.[1] In particular, smectite clays pillared by metal oxides have been used successfully as acid catalysts in several reactions such as the dehydration of alcohols,[2] conversion of methanol to hydrocarbons,[3] petroleum cracking[4] and production of fine chemicals.[5] Initially, the polyoxocationic species of aluminium,[6,7] zirconium[8] and titanium[9] were used to prepare the pillared clays. No doubt the polynuclear hydroxy metal ions formed by hydrolysis in aqueous solutions can yield stable pillared clays with interlayer free spacings in the range 5–20 Å, but the disadvantage is that only a limited number of metals can form the oligomeric species. Therefore suitable metal chelates of Fe,[10] Cr,[11] Rh,[12] Nb[13] and Hg[14] *etc.* were used as pillaring species. Of these metal chelates, iron and chromium give rise to thermally stable (up to 500 °C) oxide pillars. Although many studies have been carried out on the above transition-metal oxide pillared clays, no reports are available on manganese(IV) oxide pillared clays except our patented document[15] where the μ-oxo tris-aquo trinuclear manganese(III) acetate complex, which itself is a good redox catalyst,[16] was used as the pillaring agent.

As far as the general preparation is concerned, only Na-exchanged clays have been used extensively as the starting material, although the acid-activated clay itself is more acidic and catalytically active.[17] Preliminary work with low-temperature catalysis showed that acid treatment before pillaring has a beneficial effect.[18,19] In our earlier work, we have also reported that iron oxide pillared clays prepared from acid-activated montmorillonites showed improved Brønsted and total acidity compared to the materials prepared from Na-exchanged clay.[20] With this in mind we have used both acid-activated and Na-exchanged clays in the present work. This paper deals with the comparative studies on the preparation and characterisation of the novel manganese(IV) oxide pillared montmorillonite prepared from both clays using a trinuclear manganese(III) acetate complex as a precursor for the pillaring agent.

† Part 1, ref. 20.

Experimental

Materials and chemical analysis

The parent montmorillonite (Mainburg, Germany) and acid-activated montmorillonite (chemical composition as in Table 1) were used as the starting materials. The parent clay was exchanged with NaCl before pillaring. Acid activation was carried out using sulfuric acid at 95 °C for 15 h, according to Bovey and Jones.[21] The clay was treated with a sulfuric acid solution, whilst maintaining a constant clay concentration of 20 ml g^{-1} and an acid to clay ratio of 0.3 (m/m). The cation-exchange capacities of the air-dried NaMont and HMont were found to be 86 and 65 mequiv $(100\ g)^{-1}$, respectively. The trinuclear manganese(III) acetate complex, $[Mn_3O(COOCH_3)_6(H_2O)_3]^+CH_3COO^-$, prepared according to Andrulis *et al.*,[22] was used as the pillaring agent. As the complex is stable in methanol and glacial acetic acid, both these solvents were used separately for ion-exchange experiments. Cation exchange was carried out from a fixed volume of complex and clay suspension, with the complex to clay ratio being varied from 2 to 20 mmol g^{-1}, following the detailed method reported elsewhere.[15] In addition to the samples prepared by a single-step ion-exchange process, samples were also prepared using multistep ion-exchange processes using both the starting materials, taking 1 mmol g^{-1} of clay each time. The resulting samples were filtered, washed and dried at room temperature. The air-dried samples were calcined at 110, 300,

Table 1 Chemical compositions of parent and acid-activated montmorillonites dried at 120 °C

composition	parent montmorillonite (%)	acid-activated montmorillonite (%)
SiO_2	62.0	72.0
Al_2O_3	19.8	14.5
Fe_2O_3	4.2	3.0
CaO	3.3	2.3
MgO	4.8	3.2
Na_2O	0.8	0.5
K_2O	1.8	1.4
H_2O	*ca.* 3.2	*ca.* 3.0

400 and 500 °C, collected in air-tight bottles and stored in a desiccator for further study. Total manganese contents in the complex and in the pillared materials were estimated by atomic absorption spectroscopy (AAS).

Textural properties

The XRD patterns of the oriented pillared clay samples on glass slides were recorded on a Philips semiautomatic diffractometer using a Cu-Kα radiation source and an Ni filter in the range $2\theta = 2$–$20°$. From the d_{001} values, basal spacings were calculated. Adsorption of ethane-1,2-diol vapour was also carried out on the same samples to examine for any further changes in basal spacings.

TG–DSC analyses of the room-temperature dried samples were carried out in dry air using a Stanton Redcroft (STA 625) thermal analyser in the temperature range 30–600 °C at a heating rate of 10 °C min^{-1}.

IR spectra of the original samples and of the ammonia-adsorbed samples were recorded with a Jasco FTIR spectrometer in the range 4000–400 cm^{-1} using the KBr disk method. All the samples were degassed at 120 °C in vacuum (1×10^{-4} Torr) before analysis.

Surface areas (BET), pore volumes, average pore diameters and pore size distributions were determined by the nitrogen adsorption–desorption method at liquid-nitrogen temperature using a Quantasorb instrument (Quantachrome, USA). Prior to adsorption–desorption measurements, all the samples were degassed at 120 °C and 10^{-5} Torr for 5 h. Since no current theory is able to describe micropore filling mathematically,[23] the more generalised standard isotherm method was used to estimate the extent of microporosity.[23–25] Since the validity of the *t*-plot based on the *C* values of the BET equation has been criticised, the use of the α_s plot, defined as $\alpha_s = (n/n_s)_{ref}$ (n_s is the amount adsorbed by the reference solid at $P/P_0 = s$) has been proposed.[23,26] According to Sing[27] it is convenient to place $\alpha_s = 1$ at $P/P_0 = 0.4$, since monolayer coverage and micropore filling occurs at $P/P_0 < 0.4$, while capillary condensation takes place at $P/P_0 > 0.4$. But the difficulty associated with the application of the α_s method is the need for a non-porous reference solid with the same surface structure. In this work Na-montmorillonite is taken as the reference material with the assumption that it has no microporosity. Although this material has some measurable pores in the mesopore range, it will not affect the measurement when used as a reference material.

Surface acidity

In addition to the IR method, surface acidity was also determined spectrophotometrically[28] on the basis of irreversible adsorption of organic bases such as pyridine (py), piperidine (pp) and 2,6-dimethylpyridine (dmpy). In all cases, adsorption was carried out in cyclohexane solution at 298 K according to the detailed procedure described previously.[28,29]

Results and Discussion

Intercalation

The uptakes of the trinuclear Mn^{III} acetate complex by both clays are shown in Fig. 1. This shows that the uptake of Mn^{III} increases with concentration in the solution up to 10 mmol g^{-1}, and thereafter decreases with further increases in concentration. Preliminary experiments show that a very low uptake of Mn^{III} takes place in glacial acetic acid (curve A) compared to methanol (curves B and C). Therefore, for further studies, the samples were prepared from methanol media. It is also observed from the plot that uptake of Mn^{III} in the case of the acid-activated clay was low in comparison to the Na-exchanged clay. This type of observation was also found in the case of

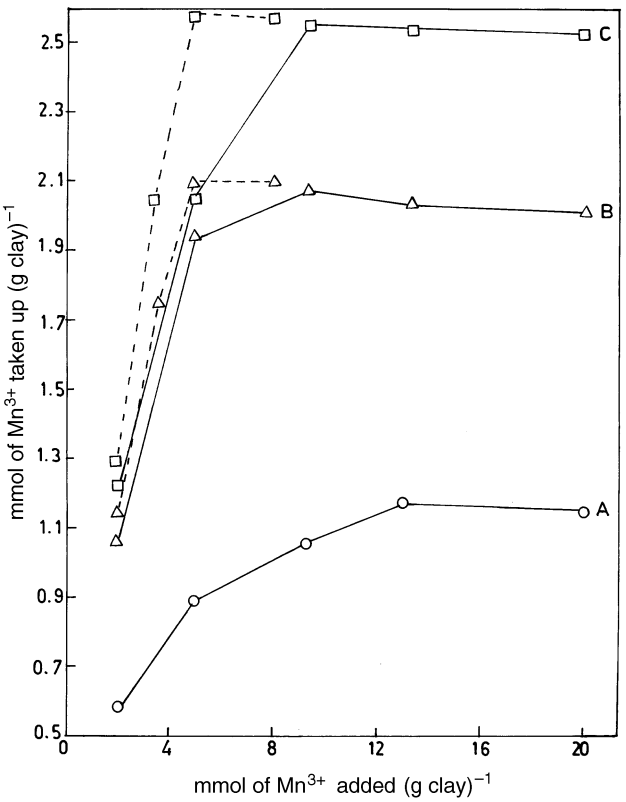

Fig. 1 Uptake of Mn^{III} by (A) Na-exchanged montmorillonite in glacial acetic acid, (B) acid activated montmorillonite in methanol, (C) Na-exchanged montmorillonite in methanol. Dotted line shows the multistep ion-exchange process while the solid line shows the single-step process.

the Fe^{III} pillared clay in our earlier study,[20] which can be correlated to the partial deformation of the clay layer and the reduction of the cation-exchange capacity of the clay owing to the acid treatment. Interestingly, better intercalation was found when stepwise ion exchange was carried out, taking in 1 mmol g^{-1} of Mn^{III} each time and repeating five times, than the single-step process (taking 10 mmol g^{-1} of complex). This shows the advantage of the multistep ion-exchange process over the single-step process. Tables 2 and 3 show that the basal spacings and surface areas are directly proportional to the amount of Mn^{III} uptake, which increased to 10 mmol (g clay)$^{-1}$ of Mn^{III} in the suspension. This shows that the opening up of the clay layer depends upon the amount of complex intercalated. However, when the complex to clay ratio in the suspension was increased to >10 mmol g^{-1}, the basal spacings and the surface areas decreased although there was little decrease in the Mn^{III} uptake. So it seems that intercalation is less favoured at higher Mn^{III} concentrations. This indicates that the total amount of the complex present in the pillared materials is not due to intercalation; rather, a portion of it is adsorbed on the surface which results in the low basal spacing. These adsorbed complexes probably block the pores and thus decrease the surface area. However, the samples (Mn-NaMont-5s and Mn-HMont-5s) prepared by the stepwise ion-exchange process (5 mmol g^{-1}) show the highest surface areas and basal spacings of both clays. These two samples only were used for further comparison purposes.

Textural properties

Table 4 shows that the d_{001} basal spacings of the Mn-NaMont-5s and Mn-HMont-5s samples decrease with increasing calcination temperature. However, both samples were stable up to 500 °C, having gallery heights of 7.5 and 7.2 Å, respectively (Fig. 2). Moreover, after the adsorption of ethane-1,2-diol,

Table 2 Manganese uptakes, surface areas and basal spacings with changes in the complex to clay ratio for acid-activated montmorillonite

sample	sample code	Mn^{III} added/ mmol g^{-1}	Mn^{III} in solution/mol l^{-1}	Mn in pillared sample (mass%)	surface area/m^2 g^{-1}	basal spacing at 500 °C/Å
1	Mn-HMont-2	2	0.02	5.2	185	14.1
2	Mn-HMont-5	5	0.05	9.8	240	15.8
3	Mn-HMont-10	10	0.10	10.2	265	16.8
4	Mn-HMont-15	15	0.15	10.18	261	16.7
5	Mn-HMont-20	20	0.20	10.15	240	16.1
6	Mn-HMont-5_s[a]	5	0.02	10.23	268	16.8

[a]This sample was prepared by the stepwise ion-exchange process taking in 1 mmol g^{-1} of Mn^{III} each time.

Table 3 Manganese uptakes, surface areas and basal spacings with changes in the complex to clay ratio for Na-montmorillonite

sample	sample code	Mn^{III} added/ mmol g^{-1}	Mn^{III} in solution/mol l^{-1}	Mn in pillared sample (mass%)	surface area/m^2 g^{-1}	basal spacing at 500 °C/Å
1	Mn-NaMont-2	2	0.02	6.3	187	14.2
2	Mn-NaMont-5	5	0.05	10.1	245	16.3
3	Mn-NaMont-10	10	0.10	12.33	275	17.0
4	Mn-NaMont-15	15	0.15	12.30	270	16.8
5	Mn-NaMont-20	20	0.20	12.27	242	16.4
6	Mn-NaMont-5_s[a]	5	0.02	12.40	280	17.2

[a]This sample was prepared by the stepwise ion-exchange process taking in 1 mmol g^{-1} of Mn^{III} each time.

Table 4 Variation of textural parameters with calcination temperature

sample	S_{BET}/ m^2 g^{-1}	S_z/ m^2 g^{-1}	pore volume/ ml cm^{-3}	C_{BET}	basal spacing/ Å	av. pore diameter/Å	V_m[a]/ml cm^{-3}
Mn-NaMont-110	97	—	—	—	21.2	—	—
Mn-NaMont-300	252	246.8	0.2175	382	18.0	34.5	0.120
Mn-NaMont-400	274	—	—	—	17.3	—	—
Mn-NaMont-500	280	281.3	0.2355	540	17.1	33.4	0.163
Mn-HMont-110	109	—	—	—	20.4	—	—
Mn-HMont-300	241	239.8	0.2514	337	17.7	41.9	0.111
Mn-HMont-400	260	—	—	—	17.0	—	—
Mn-HMont-500	268	264.1	0.2754	434	16.8	40.6	0.137

[a]V_m is the micropore volume calculated from the α_s plot.

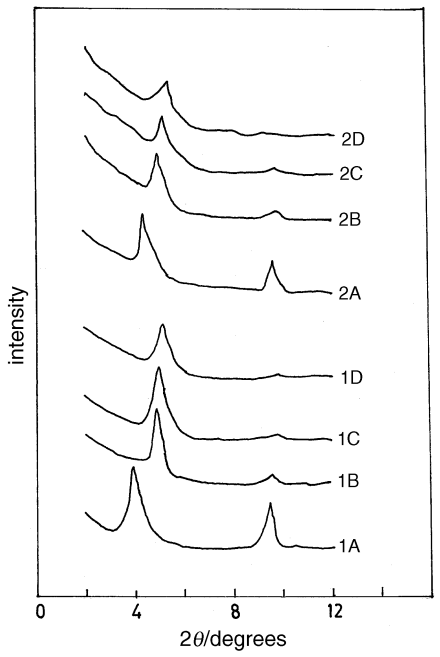

Fig. 2 Powder XRD patterns of (1) the Mn-NaMont-5 samples and (2) the Mn-HMont-5 samples calcined at (A) 110 °C, (B) 300 °C, (C) 400 °C, (D) 500 °C

both samples showed the same interlayer distances, which indicates the stabilisation of cross-linked pillars owing to strong complex–clay interactions.

TG–DSC thermograms (Fig. 3) of both samples Mn-NaMont-5s and Mn-HMont-5s show a initial endothermic peak before 150 °C, indicating the loss of interlayer and surface-adsorbed solvent molecules. The second intense exothermic peak within the 200–300 °C range indicates the decomposition of the acetyl group of the complex. However, the Mn-HMont-5s sample shows a peak at 260 °C which is higher than the equivalent peak position of Mn-NaMont-5s (254 °C). This difference in decomposition temperature is due to the difference in the opening up of the clay layers. This inverse relation of the interlayer distance with the complex decomposition temperature was also reported earlier in the case of the trinuclear Cr^{III} acetate complex pillared zirconium phosphate.[30] As the uptake of Mn^{III} is low in the case of Mn-HMont-5s, so is the percentage of mass loss owing to the decomposition of acetyl groups. Both samples showed an endothermic peak around 472 °C which may be due to the dehydroxylation of the manganese oxide pillars.

FTIR spectra of both room-temperature-dried samples (Fig. 4) show characteristic bands at 1548 and 1446 cm^{-1} corresponding to the COO^- assymmetrical (ν_{as}) and symmetrical (ν_s) stretching vibrations, respectively. The difference ($\nu_{as}-\nu_s$) of 102 cm^{-1} is characteristic of the bidentate acetate group.[31] This indicates that the intercalated complex still retains its bidentate acetate group inside the clay layer. But the samples calcined at 400 °C did not show the above charac-

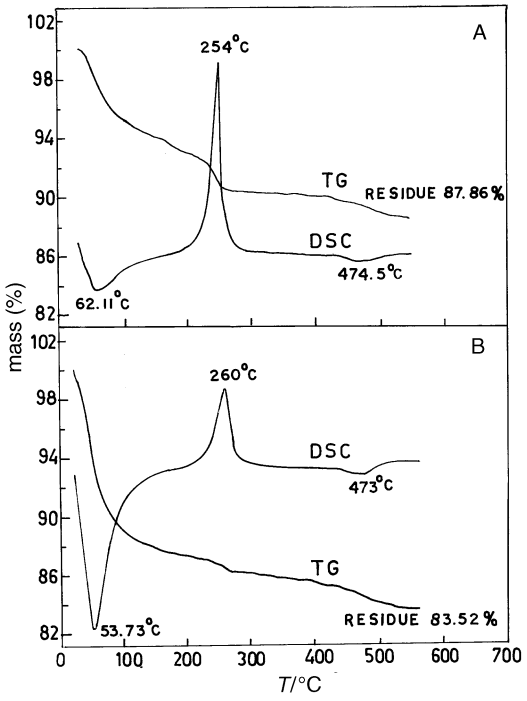

Fig. 3 TG–DSC analysis of Mn^{III} acetate pillared montmorillonite dried at room temperature: (A) 7.2 mg Mn-NaMont-5, (B) 5.9 mg Mn-HMont-5

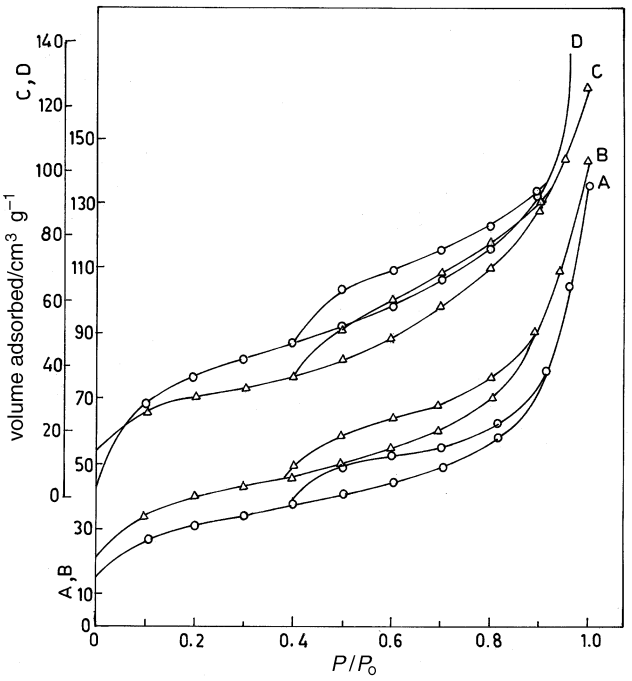

Fig. 5 Nitrogen adsorption–desorption isotherms of (A) Mn-NaMont-500, (B) Mn-NaMont-300, (C) Mn-HMont-500 and (D) Mn-HMont-300

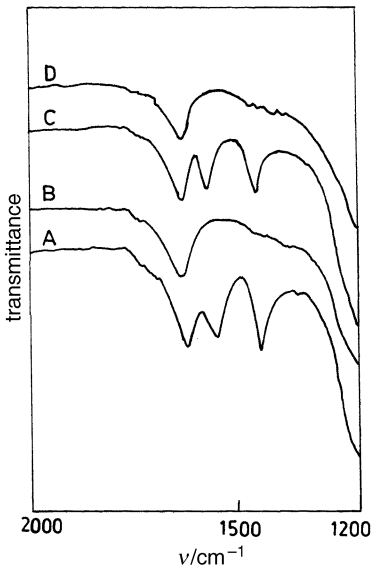

Fig. 4 FTIR spectra of (A) Mn-NaMont-RT, (B) Mn-NaMont-400, (C) Mn-HMont-RT and (D) Mn-HMont-400

teristic peak, indicating the complete decomposition of the complex forming the oxide pillar.

Changes in surface areas (BET) of both samples with respect to the calcination temperature, presented in Table 4, show the increase in surface area with increasing calcination temperature. Similarly, the pore volumes also increased with the calcination temperature. This may be due to the decomposition of the complex with increasing temperature to form the oxide pillar which generated the void micropores inside the clay layer. So the formation of micropores increased the surface area as well as the pore volumes. The complete adsorption–desorption isotherms of both samples calcined at 300 and 500 °C are presented in Fig. 5. All the curves are of nearly the same type and are of type IV in the BDDT classification.[32] The high C_{BET} values (Table 4) indicated the microporous structure of the pillared samples.[33] Assuming the pores to be cylindrical, the average pore diameters d, were calculated using the formula $d=4\ V_p/S_p$, where V_p is the pore volume and S_p is the specific internal surface area of the pores. The average pore diameters calculated by this method are given in Table 4. This shows that with increasing calcination temperature the average pore diameter decreased for both samples, which was supported by the pore size distribution data calculated using the BJH equation[34] and presented in Fig. 6.

Interestingly, the pore size distribution of the acid-activated sample showed a somewhat broader peak (average pore diameter 41 Å) whereas the Mn-NaMont-5s sample showed a sharp peak (average pore diameter 33 Å) at 500 °C calcination. This may be due to the development of mesoporosity in the clay layer during the acid treatment. However, the Mn-NaMont-5s sample calcined at 300 °C also showed two types of pores which may be due to the incomplete formation of the oxide pillar. But the sample calcined at 500 °C showed a uniform pore diameter, similar to that of the zeolite type of structure. The acid-activated material showed somewhat lower basal spacings and surface areas but possessed significantly higher total pore volumes. This increase in pore volume may be due to low manganese uptake which results in the occupation of less interlayer space. Mn-NaMont-5s samples show higher micropore volumes (V_m) in comparison to the Mn-HMont-5s samples. This shows that the micropore size is more controllable when Na-exchanged montmorillonite is used as the starting material. The α_s plots of both samples calcined at 300 and 500 °C are also presented in Fig. 7, which shows the downward deviation at high α_s values in all the cases. This downward deviation may be due to the presence of micropores or slit-like pores. Specific surface area values (S_α), calculated from the slopes of the line passing through the origin of the α_s plot [using the formula $s_\alpha=2.87(V_{ads}/\alpha_s)$], are very similar to the S_{BET} values, indicating the accuracy of the reference method (Table 4).

Surface acidities

The IR spectra of the samples with adsorbed ammonia in the region 1800–1200 cm^{-1} of both samples calcined at 300 and 500 °C are shown in Fig. 8. The relative peak height at

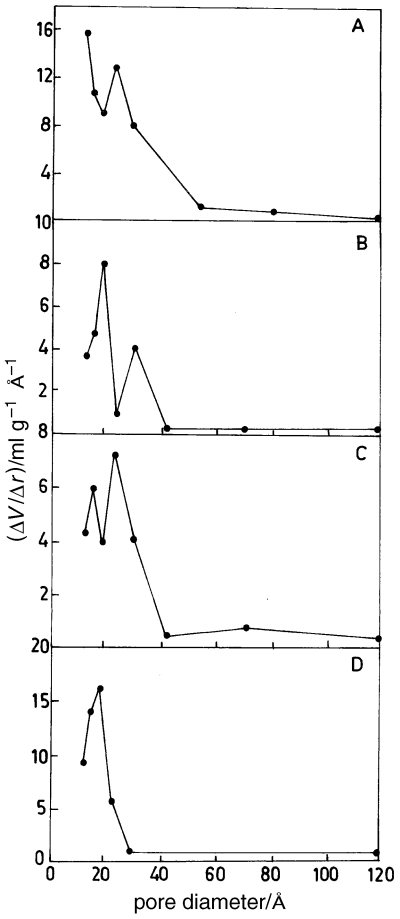

Fig. 6 Distribution of pore sizes as a function of pore diameter: (A) Mn-HMont-300, (B) Mn-HMont-500, (C) Mn-NaMont-300 and (D) Mn-NaMont-500

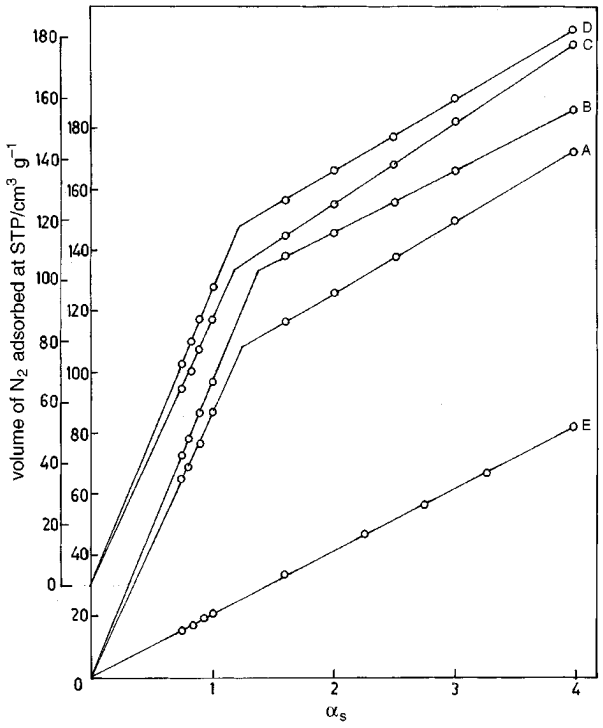

Fig. 7 α_s-plots of (A) Mn-NaMont-300, (B) Mn-NaMont-500, (C) Mn-HMont-300, (D) Mn-HMont-500, (E) Na-Mont (reference)

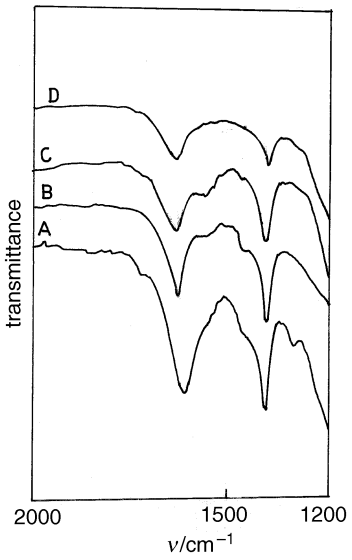

Fig. 8 FTIR spectra of ammonia adsorbed samples: (A) Mn-HMont-300, (B) Mn-NaMont-300, (C) Mn-HMont-500, (D) Mn-NaMont-500

Table 5 Surface acidities of pillared samples calcined at different temperatures

sample	T/°C	py/ μmol g^{-1}	pp/ μmol g^{-1}	dmpy/ μmol g^{-1}
Mn-NaMont-110	110	210	425	120
Mn-NaMont-300	300	570	905	260
Mn-NaMont-400	400	545	840	220
Mn-NaMont-500	500	520	670	60
Mn-HMont-110	110	215	430	135
Mn-HMont-300	300	580	955	320
Mn-HMont-400	400	550	900	270
Mn-HMont-500	500	530	720	90

1433 cm^{-1}, which corresponds to the Brønsted acidity,[35] decreased with increasing calcination temperature from 300 to 500 °C for both samples. However, the peak intensity at both calcination temperatures was higher in the case of Mn-HMont-5s, which indicates the improvement in Brønsted acidity of the sample prepared from the acid-activated montmorillonite. Both samples showed another peak at 1620 cm^{-1}, which is characteristic of both Lewis and Brønsted acid sites. In addition, the total acidities measured by the spectrophotometric method also decreased with increasing calcination temperature (Table 5). As piperidine is a base, having a pK_a value of 11.1, it measured the total acidity, while the adsorption of pyridine (pK_a = 5.3) measured only the strong acid sites. It is reported that 2,6-dimethylpyridine (dmpy) is preferentially adsorbed on the Brønsted acid sites and it can therefore be used to estimate the Brønsted sites.[36] It is observed that adsorption of dmpy in the cases of the 300 °C calcined samples are higher than those of the 500 °C calcined samples. This supports the earlier studies on pillared clays which showed that Brønsted acidity decreases to a negligible value at 500 °C.[37] Although both methods show that the acidity is low for the 500 °C calcinated samples, they still retain some of the Brønsted acid sites, particularly in Mn-HMont-5s. This shows the importance of the use of the acid-activated clay for the preparation of acidic pillared clays. The acidities of the manganese(IV) oxide pillared materials prepared from both types of montmorillonites are somewhat low in comparison to those of the Cr^{III} and Fe^{III} oxide pillared materials.[20,38]

Conclusions

It is possible to synthesise high surface area (281 m^2 g^{-1}), thermally stable (up to 500 °C) manganese oxide pillared

montmorillonite by intercalation of a trinuclear manganese(III) acetate complex in methanol. For this material both Na-exchanged and acid-activated clays can be used as the starting material. Although the materials prepared using the acid-activated clay showed somewhat lower uptakes of the complex, basal spacings and surface areas in comparison to those prepared from the Na-exchanged clay, they possess significantly higher pore volumes. In addition, this material prepared from the acid-activated clay shows the presence of both micropores and mesopores while the other material possesses predominantly uniform pores. So the formation of micropores is controlled more readily when the Na-exchanged montmorillonite is used. As far as the acidity is concerned, the acid-activated montmorillonite is much more useful in increasing the total and the Brønsted acidity of the pillared material, making it a potential solid-acid catalyst.

We are thankful to Prof. H. S. Ray, Director, Regional Research Laboratory, for his permission to publish this paper and Dr. S. B. Rao, HOD, IC group, for his constant encouragement and inspiration throughout the work. T. M. is thankful to CSIR, New Delhi for the award of SRF.

References

1 *Pillared Layered Structures: Current Trends and Applications*, ed. I. V. Mitchell, Elsevier, London, 1990.
2 R. Birch and C. I. Warburton, *J. Catal*., 1986, **97**, 511.
3 Toyo Soda Mfg. Co., *Jpn. Pat*., JP 8083635, 1983.
4 F. Figueras, *Catal. Rev. Sci. Eng*., 1988, **30**, 456.
5 J. M. Adams, *Appl. Clay Sci*., 1987, **2**, 309.
6 S. Yamanaka and G. W. Brindley, *Clays Clay Miner*., 1987, **26**, 21.
7 M. L. Ocelli and R. M. Tindwa, *Clays Clay Miner*., 1983, **31**, 22.
8 G. J. J. Bartley and R. Burch, *Appl. Catal*., 1985, **19**, 175.
9 J. Sterte, *Clays Clay Miner*., 1986, **34**, 658.
10 M. A. Martin-Luengo, H. Martins-Carvalho, J. Ladriere and P. Grange, *Clay. Miner*., 1989, **24**, 495.
11 A. Jimenez-Lopez, J. Maza-Rodriguez, P. Olivera-Pustor, A. Maireles-Torres and E. Rodriguez-Castellon, *Clays Clay Miner*., 1993, **41**, 328.
12 T. J. Pinnavaia and P. K. Welty, *J. Am. Chem. Soc*., 1975, **97**, 3819.
13 S. P. Christiano, J. Wang and T. J. Pinnavaia, abstract from *19th Annual Meeting of the Clay Minerals Society*, Hilo, Hawaii, 1982.
14 F. Tsvetkov and J. White, *Chem. Mater*., 1989, **1**, 149.
15 K. M. Parida, T. Mishra and S. B. Rao, *Ind. Pat*. application.
16 J. R. Gilmore and J. M. Mellor, *J. Chem. Soc. C*, 1971, 2355.
17 R. W. McCabe, in *Inorganic Materials*, ed. D. W. Bruce and D. O'Hare, Wiley, Chichester, 1992, p. 296.
18 R. Mokaya and W. Jones, *J. Chem. Soc*., *Chem. Commun*., 1994, 929.
19 R. Mokaya and W. Jones, *J. Catal*., 1995, **153**, 76.
20 T. Mishra, K. M. Parida and S. B. Rao, *J. Colloid Interface Sci*., 1996, **182**, in press.
21 J. Bovey and W. Jones, *J. Mater Chem*., 1995, **5**, 2027.
22 P. J. Andrulis, P. J. Dewar, R. Dietz and R. L. Hunt, *J. Am. Chem. Soc*., 1966, **88**, 5433.
23 K. S. W. Sing, D. H. Eerett, R. A. W. Haul, L. Moscou, R. A. Pierotti and J. Rouquerol, *Pure Appl. Chem*., 1985, **57**, 603.
24 J. Seifert and G. Emig, *Int. Chem. Eng*., 1991, **31**, 29.
25 A. Lecloux, *Mem. Soc. R. Sci. Liege, Ser. 6 1971*, vol. 1, p. 4 169.
26 S. J. Gregg, in *Adsorption at the gas–solid and liquid–solid interface*, ed. J. Rouquerol and K. S. W. Sing, Elsevier, Amsterdam, 1982, p. 153.
27 K. S. W. Sing, in *Surface Area Determination*, ed. D. H. Everett and R. H. Ottewill, Butterworths, London, 1970, p. 25.
28 K. M. Parida, P. K. Satapathy, A. K. Sahoo and N. N. Das, *J. Colloid Interface Sci*., 1995, **175**, 112.
29 K. M. Parida and T. Mishra, *J. Colloid Interface Sci*., 1996, **179**, 233.
30 P. Maireles-Torres, P. Oliver-Pastor, E. Rodriguex-Castellon, A. Jumenez-Lopez and A. A. G. Tomlinson, *J. Mater. Chem*., 1991, **1**, 739.
31 K. Nakamoto, *Infrared and Raman Spectra of Inorganic and Coordination Compounds*, 4th edn., Wiley, New York, 1986.
32 S. Brunauer, D. W. Demming, L. S. Demming and E. Teller, *J. Am. Chem. Soc*., 1940, **62**, 1723.
33 S. J. Gregg and K. S. W. Sing, *Adsorption, Surface Area and Porosity*, 2nd edn., Academic Press, London, 1982.
34 E. P. Barret, L. G. Juyner and P. P. Halenda, *J. Am. Chem. Soc*., 1951, **73**, 373.
35 M. R. Basila and T. R. Kantner, *J. Phys. Chem*., 1967, **71**, 467.
36 H. C. Brown and R. B. Johanneson, *J. Am. Chem. Soc*., 1953, **75**, 16.
37 D. Tichit, F. Fajula, F. Figueras, C. Guegen and J. Bousquet, *Am. Chem. Soc. Div. Pet. Chem.,* 1987, **32**, 647.
38 T. Mishra, K. M. Parida and S. B. Rao, *J. Catal*, submitted.

Paper 6/03797F; *Received* 31*st May*, 1996